Automated Shape Classification of Buried Objects with Low Frequency Multistatic Sonar

Monica Montanari, Joseph R. Edwards, and Henrik Schimdt
Massachusetts Institute of Technology
Department of Ocean Engineering
77 Massachusetts Avenue
Cambridge MA 02139 USA
momo@mit.edu

Abstract— **In this paper a novel and simple technique is presented that exploits multi–platform sonar capabilities for automated target shape classification. This technique is based on the relation between the target beampattern and the size and shape of the object. The performance are evaluated in terms of mean square error of the size estimator and probability of correct classification. This technique is shown to offer improved performance and lower computational load and physical constraints compared to the imaging–based classification techniques.**

I. Introduction

Concurrent target detection and classification is important for reducing the false alarm rate and increasing the effective area coverage rate of a mine hunting sonar system. One approach to achieve this purpose is to deploy multiple receiver vehicles to acquire the active sonar signal of a single off–shore platform source. Such an unmanned vehicle system is capable of exploiting the spatial signatures of the buried targets and reconstruct their acoustic scattering characteristics. The target detection task is exploited by using adaptive techniques with the help of a tracking algorithm, which decreases the occurrence of false alarms [1]. Once a possible target is tracked by the system, the classification algorithm identifies details in the scattered field that can be used to discriminate between objects. To this purpose, different adaptive processing techniques are employed, involving target and reverberation modeling.

Monostatic imaging concepts are extensively used in the sonar community to aid target detection and classification [2], but these applications have some fundamental limitations in autonomous systems due to resolution limits and physical system restrictions. High frequency sonar systems, such as those typically employed for proud targets, are inhibited in buried target applications by the high attenuation rate of the sediment as the incident pulse propagates through the seabed to the buried target. This attenuation imposes a reduction in the design frequency of the sonar system, which leads to an increased aperture length requirement to achieve the same resolution. While synthetic aperture sonar (SAS) has been successful in providing improved resolution at reduced frequencies [3], [4], the processing requirements and sensor dedications for platform motion correction, image construction and image–based classification are extremely demanding [5]- particularly in applications that require unsupervised or autonomous vehicle operations. In addition, image–based classification from multiple vantage points requires extended time due to time–sharing of the waveguide among the multiple sources, as well as a high rate of information exchange between vehicles, which is difficult to support in a coastal environment.

In order to mitigate these problems, new adaptive shape classification techniques, which are based on multistatic measurements of the target spatial signature, are investigated in this paper. The spatial response of a target is measured over various bistatic angles to estimate a planar cut of the 3–D scattered field of the target. Main lobes of the scattered field indicate the characteristic dimension and aspect angle of the target. Multiple vehicles exchange only a series of scattering angles and scattering amplitudes to reconstruct the full field. Such shape classification techniques are based on a parametrization of the problem and lead to a significant reduction in processing and implementation requirements.

The reconstruction accuracy and the signal to noise ratio (SNR) requirements are compared with the state–of–the–art monostatic imaging techniques. Estimation performance is extensively assessed by calculating the statistical bias, variance and mean square error (mse) of the estimators for different SNR scenarios, target characteristic dimensions and reverberation correlation.

Under some assumption about the statistical nature of the reverberation, the maximum likelihood estimator (MLE) can be easily derived and its performance evaluated and compared to the Cramér–Rao lower bound (CRLB). A robustness analysis is also conducted when the assumption are not completely validated and the consequent performance degradation is evaluated in order to encourage the employment of other alternative sub–optimal estimators, which can be more easily derived when the statistics of the reverberation does not match the model, or the model itself is unknown. Finally, it is shown how a broadband transmitter can be employed in order to increase the probability of detection with respect to the narrowband case.

II. Target Shape Estimation

Consider a target positioned at the center of the reference system axes, as in Fig. 1, at a depth D from the sea surface. In the far field of the target consider a sonar transmitter on board of a single AUV, which insonifies the target, and multiple receivers on board of different vehicles, which move on specific trajectories. Due to the far field assumption, the target radiates in the space a pressure field

described by the beampattern $\beta(\theta, \phi)$:

$$P_T(k, R, \theta, \phi) = \frac{e^{jkR}}{R}\beta(\theta, \phi) \quad (1)$$

where $k = 2\pi/\lambda$ is the wavenumber, with $\lambda = c/f$ denoting the wavelength, c the sound speed and f the frequency, R is the target–receiver distance and $\beta(\theta, \phi)$ is the beampattern, which depends only on the target–receiver polar and azimuthal angles, respectively θ and ϕ. When a planar cut of the beampattern is considered, the dependence on the polar angle θ is released. Each AUV measures a set of angles–amplitudes $(\phi, |P_T(k, R, \phi)|)$ in the backward scattering direction, which represents a sampling of the 3–D planar cut of the beampattern. From this information it is possible to reconstruct the characteristic dimension of the target, which is related to the dimension of the main lobe in the beampattern.

In this paper two different types of targets are considered: elongated targets (i.e. cylinders) and round targets (i.e. spheres). For the first type of targets the processing uses an analytical expression which relates the beampattern to the length of the cylinder. In this case the problem is parameterized and analytical solutions can be found depending on the various degrees of knowledge of the reverberation process. The problem is highly simplified because the degrees of freedom are strongly reduced and the probability of classification is evaluated in term of mse of the length estimator and compared to the classical CRLB.

In the case of round or arbitrarily–shaped targets, an analytical expression for the beampattern is not available, so it is necessary to use target scattering models to calculate candidate sets of angles–amplitudes to which the sampled set must be compared. The target is classified as the one who gives rise to the minimum mean square error between the sampled beampattern and the candidate ones. In the case of a sphere of radius a, if the transmitter is narrowband with central frequency f_0, then there will be a mid–range of values ka for which it is possible to distinguish the beampatterns related to different radii. On the contrary, for values of ka outside the range, the backscattered beampattern is uniform and does not depend on the sphere radius. At low ka the sphere is point-like and at high ka the returns are highly specular and thus are uniformly distributed in angle due to the shape of the sphere. For more general target shapes, the low ka regime is very similar to that of the sphere, but the high ka varies depending upon insonified face of the target.

Figure 2 shows the scattering beampatterns of two types of targets, as computed from analytical models. In both polar plots the source consists of a monofrequency plane wave arriving from the left of the figure. In Fig. 2 (a) is the resulting scattering beampattern of a cylinder with a 70^{deg} aspect angle with respect to the incoming wave. Fig. 2 (b) shows the scattering beampattern from a sphere. Note that the forward–scattering lobe cannot be exploited because this is the "blast–out" region in which the target scattering is indistinguishable from the forward scattering of the seabed.

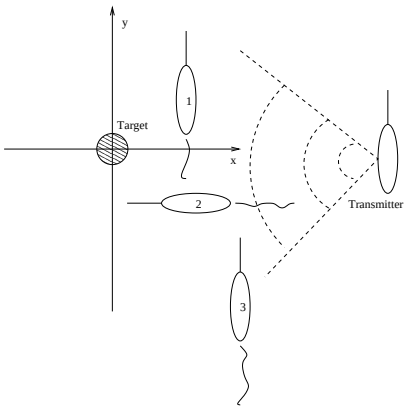

Fig. 1. Typical mission geometry with one transmitter and multiple receivers.

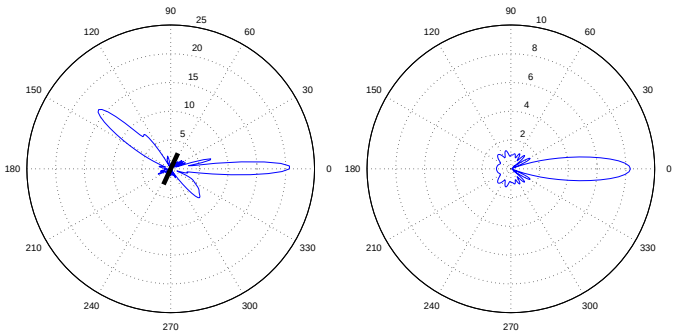

(a) Cylinder@70 deg, kL=3 (b) Sphere, ka=12.5

Fig. 2. Scattering beampatterns of canonical targets. The source is to the left, at 180 degrees.

When the transmitter is broadband, the processing involves a filter bank, where each filter is centered on a specific frequency f_k. In this case for each candidate target there exists a set of beampatterns, each of which is computed with a specific frequency, as in the narrowband case. As is shown in Section III-B, the increased availability of independent data points is used to increase the system performance.

A. Elongated Targets

Consider a cylinder of length L and radius $a << L$, with the main axis aligned with the y–axis as it is shown in Fig. 1. The receiving vehicles sample the backscattered signal at the ping rate pr and extract the beampattern amplitude from the complex envelope of the signal. The data are a set of bistatic angles–amplitudes pairs. At this processing point, the position of the target has already been estimated, so that the range R is known. In this simple case, the beampattern has a sinc–shaped function:

$$\beta(\phi) = \text{sinc}\left(\frac{L}{\lambda}\sin(\phi)\right) \quad (2)$$

where the angle ϕ is the azimuth. This expression for the beampattern is valid when the incident wave propagation direction and the main cylinder axis are orthogonal.

When the cylinder is rotated with respect to the propagation direction, or equivalently the propagation direction is $\phi_T \neq 0°$, the beampattern assumes the following form:

$$\beta(\phi) = \text{sinc}\left(\frac{L}{\lambda}\left(\sin(\phi) - \sin(\phi_T)\right)\right) \tag{3}$$

where ϕ_T denotes the steering direction. Consider the case $\phi_T = 0°$ and denotes with $R(\phi)$ the the distance between the axes origin and the AUV. The received signal amplitude is expressed as

$$s(\phi) = \frac{\beta(\phi)}{R(\phi)} = \frac{\text{sinc}\left(\frac{L}{\lambda}\sin(\phi)\right)}{\sqrt{\frac{D^2}{\cos^2(\phi)} + h^2}} \tag{4}$$

where D is the horizontal (i.e. in the $x-y$ plane) distance between the AUV and the target and h is the difference between their z–axis components. If the AUV is flying on a straight path, the sampling points are $d = v \cdot pr$ far away, where v is the AUV speed. The signal $s(\phi)$ is sampled at the positions

$$\phi_n = \tan^{-1}\left(\frac{D}{-D\frac{\lambda/L}{\sqrt{1-(\lambda/L)^2}} + (\delta+n)d}\right) \tag{5}$$

where $n = 0, 1, \ldots, N-1$ and

$$N = \frac{2D}{d\sqrt{(L/\lambda)^2 - 1} + 1} \tag{6}$$

is the maximum number of points inside the beampattern main lobe. In (5)

$$-D\frac{\lambda/L}{\sqrt{1-(\lambda/L)^2}} + \delta d \triangleq y_0 \tag{7}$$

is the first sampling point, assuming that the AUV is flying along the positive y–axis direction. Here δ is a random variable with uniform distribution in the range $[0, 1]$. Eq. (4) and (5) give the theoretical relation between the beampattern and the object length. This parameterization is the key to invert the relation in a simple way and estimate L directly.

The complete statistical signal model must account for the reverberation process, so the received signal (after beamforming and filtering) can be written as

$$\mathbf{z} = \mathbf{s}(L) + \mathbf{r} \tag{8}$$

where $\mathbf{z} = [z(0)\ z(1)\ \cdots\ z(N-1)]^T$ is the vector comprising the signal samples and $\mathbf{s}, \mathbf{r}$ are defined in the same way. If the reverberation probability density function (pdf) $p_r(\mathbf{r})$ is known, the optimum MLE can be derived as

$$\hat{L}_{ML} = \arg\max_L \{p_r(\mathbf{z} - \mathbf{s}(L); L)\}. \tag{9}$$

The MLE $\hat{L}_{ML}$ can be easily derived when the reverberation pdf is Gaussian:

$$\hat{L}_{ML} = \arg\min_L ||\mathbf{z} - \mathbf{s}(L)||^2 \tag{10}$$

where $||\cdot||$ is the vector norm operator. Because the function is non–linear, it is necessary to use numerical technique to find the zero of the derivative of the function itself. A more realistic model of the reverberation process is the K distribution [6]. The estimator cannot be derived in a closed form for K–distributed clutter, but the maximization problem can be solved with numerical algorithm. When the reverberation pdf is not Gaussian, the estimator in (10) is no longer the MLE, but rather the least squares estimator (LSE). Of course, when the reverberation is Gaussian distributed the two estimators coincide. A performance degradation is expected when the LSE is used and the reverberation is not Gaussian distributed, in fact the estimator is sub–optimal.

The estimator performance is evaluated in terms of bias $b(\hat{L}/\lambda)$ and mse of the cylinder length normalized to the wavenumber, in order to obtain non–dimensional quantities:

$$b(\hat{L}/\lambda) = E\{\hat{L}/\lambda\} - L/\lambda \tag{11}$$

$$mse(\hat{L}/\lambda) = E\{(\hat{L}/\lambda - L/\lambda)^2\} = var\{\hat{L}/\lambda\} + b^2(\hat{L}/\lambda) \tag{12}$$

where $E\{\cdot\}$ denotes the statistical expectation and $var\{\hat{L}/\lambda\} = E\{(\hat{L}/\lambda - E\{\hat{L}/\lambda\})^2\}$ is the statistical variance. In Section III-A these quantities are evaluated numerically through Monte Carlo simulations and the mse is compared to the CRLB, which is the lower bound for any unbiased estimator:

$$CRLB(L/\lambda) = \frac{1}{-E\left\{\frac{\partial^2 \ln p_r(\mathbf{z}-\mathbf{s};L/\lambda)}{\partial^2 L/\lambda}\right\}} \tag{13}$$

The lower the squared bias, the closer the mse is expected to match the CRLB, which is reported in the simulation plots as a benchmark. When the reverberation is Gaussian distributed with zero mean the CRLB can be expressed as [7]

$$CRLB(L/\lambda) = \frac{1}{\left(\frac{\partial \mathbf{s}(L/\lambda)}{\partial L/\lambda}\right)^T \mathbf{C}^{-1} \left(\frac{\partial \mathbf{s}(L/\lambda)}{\partial L/\lambda}\right)} \tag{14}$$

where $\mathbf{C} = E\{\mathbf{r}\mathbf{r}^H\}$ is the covariance matrix of the reverberation process. Usually $\mathbf{C}$ is not known and must be estimated from secondary data, i.e. data collected when there is no target present in the insonified field. The region from where the secondary data are collected must be close to the target field in order to assure the same statistical properties.

B. Round Targets

In the more general case when the shape of the target is unknown, the measured signal is compared to a set of beampatterns corresponding to different candidate objects, which are different in shape, as well as in size. A least squares criterion is used to choose which of the candidates is more close to the real target. Denote with $\beta_i(\phi_n)$ the beampattern of the i–th object, with $i = 1, \ldots, M$ and M is the number of candidate objects. Again $n = 0, \ldots, N-1$

denotes the sample number. In the backward scattering region it is $\pi \leq \phi \leq 3/2\pi$. For a narrowband transmitter the error for object i is computed as

$$\epsilon_i = \sum_{n=0}^{N-1} \left(z_{rc}(\phi_n) - \beta_i(\phi_n)\right)^2 \tag{15}$$

where $z_{rc}(\phi_n)$ is the received signal after range compensation. In order to compare the shape of the beampattern, the signals are normalized. The target is selected as the one which minimize the errors ϵ_i:

$$\bar{i} = \arg\min_i \epsilon_i \rightsquigarrow \hat{T} = T_{\bar{i}}. \tag{16}$$

The algorithm performance is evaluated by means of the probability of correct classification P_C:

$$P_C = Prob\{\hat{T} \equiv T\}. \tag{17}$$

When the transmitter is broadband, the algorithm is written as:

$$\bar{i} = \arg\min_i \sum_{k=1}^{K} \sum_{n=0}^{N-1} \left(z_{rc}^k(\phi_n) - \beta_i^k(\phi_n)\right)^2 \rightsquigarrow \hat{T} = T_{\bar{i}} \tag{18}$$

where the superscript k denotes the k–th central frequency of the filter bank. As it is shown in the example of Section III-B, processing multiple frequencies improves the probability of classification because the number of useful data points is greater.

III. Numerical Examples

A. Cylinder

Consider a cylinder in the target field as in Fig. 1 and a single receiver flying along a straight path at a distance $D = 10$ m from the y–axis and $h = 10$ m. In the following examples the AUV speed is $v = 1$ m/s, the ping rate is $pr = 1$ sec^{-1} and the sound speed is $c = 1500$ m/s. In this example a narrowband transmission is considered, with central frequency $f_0 = 3$ KHz. The minimum target size is $|L/\lambda|_{min} = 1$, which correspond to an infinite number of sampling point inside the beampattern main lobe, while the maximum target size is $|L/\lambda|_{max} = \frac{\sqrt{9d^2+4D^2}}{3d}$, which corresponds to the case when there are only 3 sampling points inside the main lobe.

Fig. 3 shows how the number of sampling points inside the main lobe in the backward scattering direction decreases for increasing L/λ. As it was already mentioned, when $L/\lambda \to 1$ the number of sampling points tends to infinity, while when $L/\lambda \to |L/\lambda|_{max}$ the number of points is minimum. The mse is expected to increase for increasing L/λ because there are less available data to process. This consideration is validated by Fig. 4 where the mse of the MLE is plotted together with the CRLB and the best imaging resolution in absence of noise and reverberation. Best imaging resolution in this and the other examples refers to the well–known $\lambda/2$ imaging resolution limit that is theoretically achievable with synthetic aperture processing.

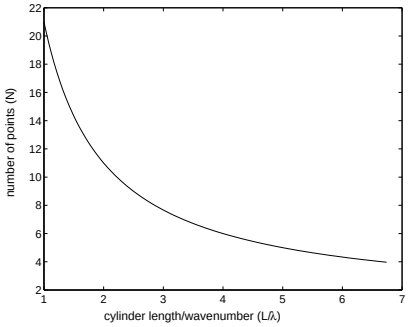

Fig. 3. Number of sampling points for different values of the normalized cylinder length L/λ (decorrelated reverberation).

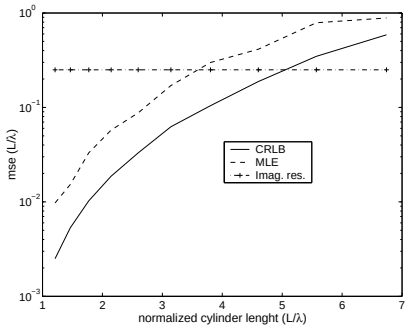

Fig. 4. Mse of the MLE compared to the CRLB and the imaging resolution for different normalized cylinder length values and $SNR =$ 10 dB (decorrelated reverberation).

The SNR is 10 dB and the reverberation is generated as a white Gaussian process. When L/λ is small enough, the MLE can significantly improve the imaging performance.

Fig. 5 shows the same quantities in function of the SNR, when $L/\lambda = 1.667$. When $SNR > 5$ dB the MLE furnishes a big improvement with respect to the best imaging techniques. When $SNR < 10$ dB the mse departs from the CRLB due to the non–linearity of the MLE.

Finally, Fig. 6 shows the mse of the MLE and the LSE as a function of the SNR, when the reverberation is an exponentially correlated Gaussian process. The correlation function is defined as

$$r(m) = E\{r(n)r(n+m)\} \tag{19}$$

and the degrees of correlation is defined through the correlation coefficient γ:

$$\gamma = \frac{r(m)}{r(m+1)}, \tag{20}$$

which for this example is chosen to be $\gamma = 3$. When the reverberation is correlated the performance degrades because the degree of innovation between adjacent samples is decreased. The performance continues to decline as the the degree of correlation increases.

B. Sphere

To evaluate the probability of classification P_C a target sphere with normalized radius $ka = 4$ is considered.

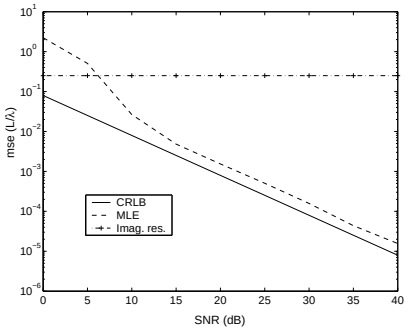

Fig. 5. Mse of the MLE compared to the CRLB and the imaging resolution for different SNR values and $L/\lambda = 1.667$ (decorrelated reverberation).

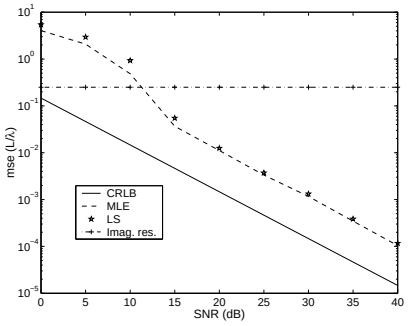

Fig. 6. Mse's of the MLE and LSE compared to the CRLB and the imaging resolution for different SNR values and $L/\lambda = 1.667$ (correlated reverberation with $\gamma = 3$).

The candidate objects are 4 cylinders with radius $a = 1$ m and normalized lengths $L/\lambda = 2, 4, 6, 8$ respectively, 4 spheres with normalized radii $ka = 2, 4, 6, 8$ respectively, and 3 manta–like truncated cones with lower radius $a_l = 1$ m, upper radius $a_u = 0.5$ m and heights $h = 2, 4, 6$ m respectively. In this example the reverberation is a white Gaussian process. Fig. 7 shows the probability of correct classification in function of SNR for the narrowband and the broadband case. For the broadband case only 2 filters are employed. Nonetheless, the probability of classification is improved compared to the single frequency case. The performance improves with the SNR and achieves probability 1 when $SNR = 5$ dB.

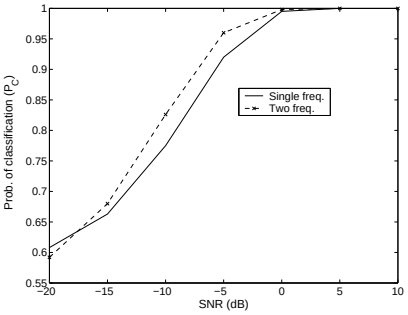

Fig. 7. Probability of classification for a target sphere in the broadband and narrowband cases, for different SNR values.

IV. Conclusions

In this paper a novel and simple technique for target shape classification is proposed. Contrary to standard classification algorithms that are based on the image of the object, this technique retrieves the object shape and size from a beampattern analysis. In the case when the beampattern function can be derived theoretically, as for a cylinder, the problem is parameterized and parametric estimation techniques are successfully employed to derive the characteristic size of the target, with the advantage of elevated performance, high processing speed and low computational load. When the target shape is unknown the algorithm involves a least squares matching method to determine the shape and size of the target between a set of candidate targets. The validity of these techniques is demonstrated through numerical examples using simulated data.

References

[1] M. Montanari, J.R. Edwards, and H. Schmidt, "Using autonomous underwater vehicles for concurrent detection and classification by means of higher–order spectral analysis," To be submitted.

[2] I. Tena Ruiz, D.M. Lane, and M.J. Chantler, "A comparison of inter–frame feature measures for robust object classifcation in sector scan image sequences," *IEEE Journal of Oceanic Engineering*, vol. 24, no. 4, pp. 458–69, 1999.

[3] M.P. Hayes and P.T. Gough, "Broad-band synthetic aperture sonar," *IEEE Journal of Oceanic Engineering*, vol. 17, no. 1, pp. 80–94, 1992.

[4] M.A. Pinto, A. Bellettini, S. Fioravanti, S. Chapman, D.R. Bugler, Y. Perrot, and A. Hetet, "Experimental investigations into high resolution sonar systems," in *MTS/IEEE Oceans'99 Conference Proceedings: Riding the Crest into the 21st Century*, Piscataway, NJ, 1999, vol. 2, pp. 916–22.

[5] A. Bellettini, S. Fioravanti, and M. Pinto, "Preliminary experimental investigation of synthetic aperture sonar micronavigation," Tech. Rep., NATO SACLANT Undersea Research Centre, La Spezia, Italy, 1999.

[6] D.A. Abraham and A.P. Lyons, "Novel physical interpretations of K–distributed reverberation," *IEEE Journal of Oceanic Engineering*, vol. 27, no. 4, pp. 800–13, 2002.

[7] S.M. Kay, *Fundamentals of statistical signal processing*, Prentice Hall, 1993.